ACS Infectious Diseases

pubs.acs.org/journal/aidcbc

Article

Hemagglutinin Stability Determines Influenza A Virus Susceptibility to a Broad-Spectrum Fusion Inhibitor Arbidol

Zhenyu Li, Tian Li, Meisui Liu, and Tijana Ivanovic*

Cite This: *ACS Infect. Dis.* 2022, 8, 1543−1552

Read Online

ACCESS | Metrics & More | Article Recommendations | Supporting Information

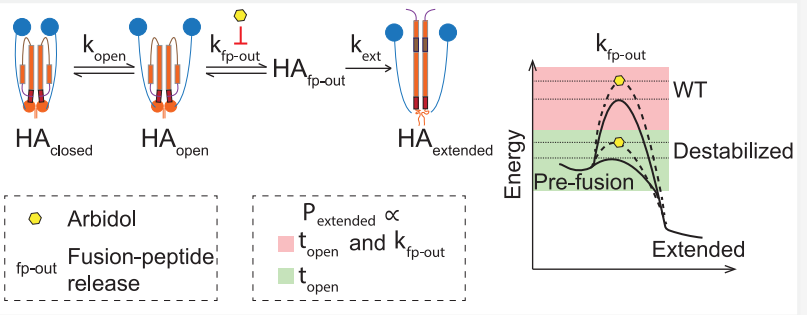

ABSTRACT: Understanding mechanisms of resistance to antiviral inhibitors can reveal nuanced features of targeted viral mechanisms and, in turn, lead to improved strategies for inhibitor design. Arbidol is a broad-spectrum antiviral that binds to and prevents the fusion-associated conformational changes in the trimeric influenza A virus (IAV) hemagglutinin (HA). The rate-limiting step during the HA-mediated membrane fusion is the release of the hydrophobic fusion peptides from a conserved pocket on HA. Here, we investigated how destabilizing or stabilizing mutations in or near the fusion peptide affect viral sensitivity to Arbidol. The degree of sensitivity was proportional to the extent of fusion-peptide stability on the prefusion HA: stabilized mutants were more sensitive, and destabilized ones were resistant to Arbidol. Single-virion membrane fusion experiments for representative wild-type (WT) and mutant viruses demonstrated that resistance is a direct consequence of fusion-peptide destabilization not requiring reduced Arbidol binding to HA. Our results support the model whereby the probability of individual HAs extending to engage the target membrane is determined by the composite of two critical forces: a "tug" on the fusion peptide by HA rearrangements near the Arbidol binding site and the key interactions stabilizing the fusion peptide in the prefusion pocket. Arbidol increases and destabilizing mutations decrease the free-energy cost for fusion-peptide release, accounting for the observed resistance. Our findings have broad implications for fusion inhibitor design, viral mechanisms of resistance, and our basic understanding of HA-mediated membrane fusion.

KEYWORDS: *influenza A virus, hemagglutinin, mechanism of membrane fusion, pH threshold, antiviral resistance, Arbidol*

To deliver their infectious cargo to the host cell, enveloped viruses mediate fusion between the viral and the target cell membranes. Membrane fusion is thermodynamically favorable but traverses a high kinetic-energy barrier upon the close approach of the fusing membranes. A homotrimeric glycoprotein, hemagglutinin (HA), serves as the catalyst for IAV membrane fusion (Figure 1A). HA is synthesized as an inactive precursor HA0 and becomes activated for fusion by cleavage into the disulfide-linked HA1 and HA2 subunits.[1] HA1 forms the globular head domain harboring the receptor binding domain and serves to stabilize the prefusion conformation of HA2. HA2 forms the highly conserved stem region and mediates membrane fusion by undergoing large-scale conformational changes triggered by low pH in late endosomes.[2] Proton binding by HA1/2 triggers HA1 head opening, which releases the constraints on HA2 conformational changes.[3,4] The extension of the central coiled-coil on HA2 (Figure 1A; B-loop-to-helix transition) projects the hydrophobic fusion peptides away from the viral membrane and toward the target membrane where they can insert.[5] Several neighboring inserted HAs (fusion cluster) cooperate during fold-back (Figure 1A; helix-to-loop transition) to overcome the kinetic-energy barrier and bring together the apposed membranes.[6] Mixing of the outer membrane leaflets in the hemifusion intermediate precedes pore opening and full fusion.[7]

Received: April 1, 2022
Published: July 12, 2022

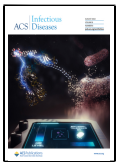

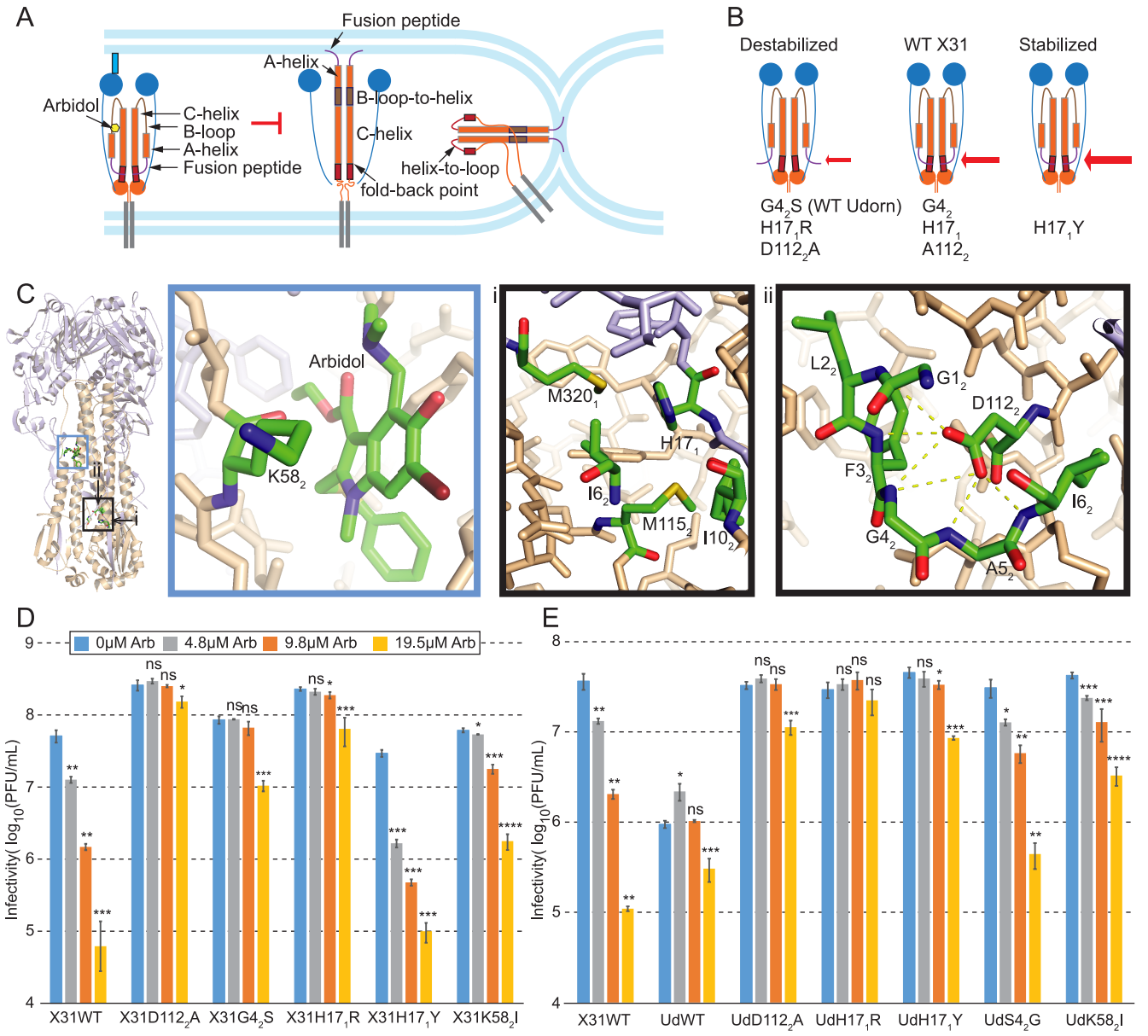

Figure 1. Destabilizing and stabilizing mutations confer Arbidol resistance and increased sensitivity, respectively. (a) A cartoon of membrane fusion-associated HA conformational changes and their inhibition by Arbidol. (b) A cartoon summarizing amino acids associated with greater or lower fusion-peptide stability. The medium red arrow indicates WT fusion-peptide stability. A larger and a smaller red arrow indicates fusion-peptide stabilization and destabilization relative to WT, respectively. The only HA2 residue where Udorn and X31 differ is position 4 with Udorn having serine and X31 having glycine. (c) Arbidol binding site (blue square) and HA region with engineered mutations (black square) are highlighted on the ribbon diagram of X31HA in complex with Arbidol (left) (PDB: 5T6N). The bound Arbidol and each of the mutated residues are separately shown as sticks in close-ups (right). The residues we are emphasizing are color-coded by atom (C-green, O-red, N-blue), and all of the other residues have all atoms in wheat for HA2 or light purple for HA1. Dashed lines show hydrogen bonds. (d, e) Results from the multicycle infectivity (plaque) assay with WT and mutant IAVs in the presence of varying concentrations of Arbidol. (d) X31HA and (e) Udorn HA. Three biological replicates were performed to derive the mean (main bars) and the standard deviation (error bars). Statistical analysis was performed using one-sided Student's t-test, comparing Arbidol-treated to untreated samples for each virus; not significant (ns), $p > 0.05$; *$p < 0.05$; **$p < 0.01$; ***$p < 0.001$; ****$p < 0.0001$.

Previous single-virion membrane fusion experiments defined how individual HAs on the virion surface contribute to the overall kinetics of hemifusion.[6−9] IAV assembles into a mixture of virion sizes from about 80 nm in diameter spheres to about 30 μm long filaments.[10,11] Depending on the virion size, about 100−10,000 densely displayed HAs interface the target membrane.[12−14] Triggered by proton binding, individual HAs extend stochastically with a rate related to the stability of the fusion peptides on the prefusion HA.[6] If HAs assume the postfusion state without engaging the target membrane, they become permanently inactivated and lost as fusion participants.[9,15] The cooperative fold-back of membrane-inserted HAs within the fusion cluster is fast, so the rate of hemifusion corresponds to the rate of cluster formation.[9] The latter rate is, in turn, defined by the rate of HA extension, the probability of HA membrane insertion versus inactivation, and the total number of activatable HAs interfacing the target membrane.[6,9,16] However, the sequence of HA conformational

https://doi.org/10.1021/acsinfecdis.2c00178
ACS Infect. Dis. 2022, 8, 1543−1552

changes leading to its extension, including HA1 opening, fusion-peptide release, and coiled-coil extension, has been a matter of debate.[5,17−23] Importantly, the relationship between HA conformational dynamics and the rate and probability of extension remains obscure.

Previous dissections of the mechanism by which broadly neutralizing antibodies binding the base of HA (base bnAbs) inhibit IAV membrane fusion led both to an updated understanding of the fusion mechanism and a model for viral persistence under external pressures.[8,9,16] Base bnAbs bind HA in the vicinity of the fusion peptide, remain bound at the pH of membrane fusion, and prevent the low pH-induced HA conformational changes.[8,16,24] Base bnAbs thus reduce the number of activatable HAs interfacing the target membrane and either delay or prevent fusion cluster formation.[8,9,16] Quantitative analysis of single-virion membrane fusion data in the presence of base bnAbs revealed that about half of the free/unbound HAs interfacing the target membrane are inactive or spontaneously inactivate over the course of the fusion reaction.[9] Despite the large noncontributing HA fraction, the probability of hemifusion remains high (close to 100%) in the absence of additional HA inactivation. A combination of cell-based and *in vitro* single-virion membrane fusion experiments with base bnAbs showed that slower fusion is inconsequential for infectivity, but lower fusion efficiency reduces the probability of productive infection.[16] A greater number of unbound HAs on filamentous virions or a greater probability of membrane insertion by the unbound HAs can enable fusion in the presence of base bnAbs.[16,25] Such a viral strategy that circumvents inhibitor effects and does not depend on mutations in the drug-binding site can be powerful in enabling resistance to inhibitors targeting the conserved, functionally constrained epitopes.

Arbidol is a broad-spectrum, small-molecule antiviral effective against a range of enveloped and nonenveloped viruses.[26−32] In the context of IAV, it binds to and stabilizes the prefusion HA inhibiting its conformational changes at low pH[27] (Figure 1A,C). More specifically, Arbidol binds to a conserved cavity about 15 angstroms away from the fusion peptide where it staples the B-loop on one HA2 monomer to the C-helix of an adjacent monomer[27] (Figure 1A,C). Arbidol binding lowers the pH threshold for HA conformational changes, likely by disfavoring HA2 coiled-coil extension. Arbidol resistance mutations, however, do not overlap its binding site, and most were shown to increase the pH threshold of HA conformational changes[26−28] (Figure S1 and Table S1). Arbidol resistance mutations overlap those of amantadine, a weak base that increases endosomal pH[33] (Table S1). This pattern of resistance suggests an indirect mechanism of Arbidol evasion despite its direct binding to HA, but the mechanistic picture is lacking.

We probed the mechanism of Arbidol resistance using our established single-virion membrane fusion platform and a panel of mutant viruses including some of the previously published Arbidol-resistant mutations[6,16,26,28] (Figure S1 and Table S1). We found that the degree of viral sensitivity to Arbidol is a direct function of fusion-peptide stability on the prefusion HA. Arbidol cannot inhibit HA conformational changes when fusion peptides are sufficiently destabilized (by mutation or pH), and it is more effective when fusion peptides are more stable. The dependence of Arbidol's effects on fusion-peptide stability is consistent with HA2 coiling near the Arbidol binding site driving and not following fusion-peptide release. Unlike base bnAbs, which prevent HA extension and inactivate bound HA, Arbidol delays HA extension and lowers its probability for only specific HA dynamics regimes. The interdependence of rate and probability of HA extension leads to a model for how premature HA inactivation is minimized. Our combined results thus establish a general mechanism of resistance to Arbidol independent of mutating its binding site and lead to a more detailed mechanistic picture of HA-mediated membrane fusion.

RESULTS

To probe the mechanism of HA resistance to Arbidol, we made a panel of viruses with mutations in HA previously shown to confer Arbidol resistance, change the pH threshold for membrane fusion, and/or change the kinetics and efficiency of membrane fusion in single-virion experiments[26−28,33−36] (Figure S1 and Table S1). Based on structural predictions, most chosen mutants either stabilize or destabilize the prefusion HA structure in or near the fusion-peptide pocket (Figure 1B,C). The only exception is the $K58_2I$ mutation, reported to stabilize HA and decrease its pH threshold for fusion, residing in the B-loop near the Arbidol binding site and about 15 angstroms away from the fusion peptide.[33,37] In addition to $K58_2I$, we chose $D112_2A$, $G4_2S$, $H17_1R$, and $H17_1Y$ mutations in the A/Aichi/68 (X31) HA background (Figures 1B,C and S1). $D112_2A$ eliminates several stabilizing hydrogen-bond interactions between the carbonyl group of $D112_2$ with the backbone atoms at the N-terminus of the fusion peptide buried deep within the fusion-peptide pocket[6] (Figure 1C). $G4_2S$ mutation in the fusion peptide also disrupts hydrogen bonding between the fusion peptide and $D112_2$ by disallowing the required fusion-peptide conformation otherwise allowed by $G4_2$[6]. $H17_1$ is located in a shallow hydrophobic pocket formed by $M115_2$, $M320_1$, $I6_2$, and $I10_2$ on the periphery of the fusion peptide near the HA surface (Figure 1C). The presence of the charged $R17_1$ would be unfavorable in this hydrophobic region and likely similar to what protonation of $His17_1$ achieves at the pH of fusion. $Y17_1$, on the other hand, would offer even greater stabilization by hydrophobic interactions and would not acquire a charge at the pH of fusion.

We additionally generated the same panel of mutations in the context of A/Udorn/72 (Udorn) HA. In both cases, the remaining segments were derived from the Udorn strain. Since WT Udorn HA already contains the destabilizing $S4_2$, we included in its context the stabilizing $S4_2G$ mutation. Some of the Udorn mutants could thus be considered double destabilizing ($G4_2S/H17_1R$) or a combination of destabilizing and stabilizing mutations (e.g., $G4_2S/H17_1Y$) for probing the dominance hierarchy of mutational effects as it relates to Arbidol sensitivity (see the Discussion section).

We measured the infectivity of our panel of mutant viruses in a standard plaque assay in the presence of a range of Arbidol concentrations from 0 to 19.5 μM (Figure 1D,E). Arbidol treatment reduced the infectivity of the WT X31HA virus to about 4- to 1000-fold in a concentration-dependent manner. All destabilized mutants in the X31HA background ($D112_2A$, $G4_2S$, and $H17_1R$) were nearly completely resistant to Arbidol (Figure 1D). A small but significant effect of Arbidol treatment was noted for only the highest Arbidol concentration, which at least in part resulted from its cytotoxicity. In fact, we could not increase Arbidol concentration in the cell-based experiments any further without causing significant cell death. Notably, the stabilizing $H17_1Y$ mutation resulted in an even greater

https://doi.org/10.1021/acsinfecdis.2c00178
ACS Infect. Dis. 2022, 8, 1543−1552

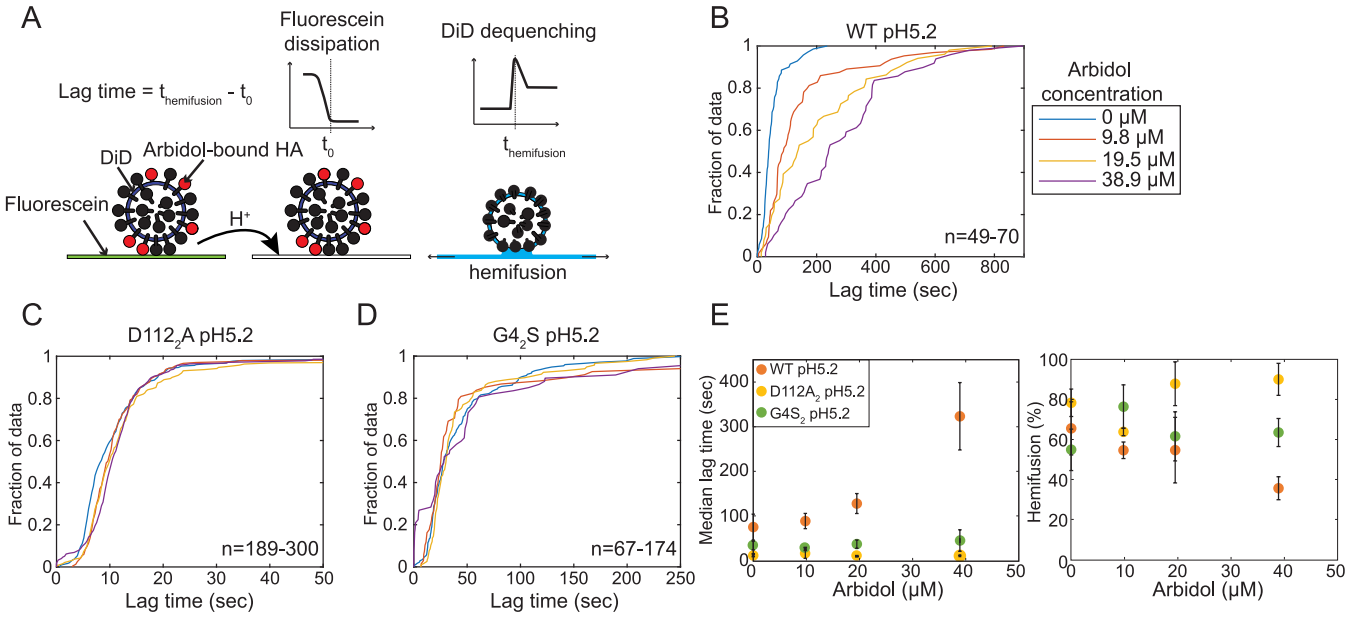

Figure 2. Destabilizing HA mutations confer Arbidol resistance to IAV in a TIRF-based single-virion membrane fusion assay. (a) Schematic of the experiment setup. Virions are preincubated with Arbidol and bound to the supported lipid bilayer via sialic acid receptors displayed on GD1a. Fluorescein on the target membrane serves as the pH sensor. DiD is incorporated into the viral membrane so that it is partially quenched. DiD dequenching indicates hemifusion between the viral and the target membranes. Hemifusion lag time is measured as the delay from fluorescein dissipation to DiD dequenching for individual virions. Hundreds of virions are recorded in each field of view. (b–d) Cumulative distributions of hemifusion lag times for X31HA WT (b), $D112_2A$ (c), and $G4_2S$ (d) mutant viruses for indicated Arbidol concentrations for representative experiments. The range for the total number (n) of virions represented by each plot is indicated. (e) Median hemifusion lag time (left) and yield (right) for X31HA WT, $G4_2S$, and $D112_2A$ viruses derived from individual experiments are plotted as the average ± standard deviation. Statistical analyses were performed using a one-sided Student's *t*-test. The *p*-values comparing median lag times of untreated to treated samples were significant for only the WT virus at 19.5 μM ($p = 0.005$) and 38.9 μM Arbidol ($p = 3.6 \times 10^{-6}$), and otherwise $p > 0.05$. The *p*-values comparing hemifusion yield between the untreated samples and 38.9 μM Arbidol were as follows: $p = 0.003$ for WT, $p = 0.046$ for $D112_2A$ (note higher efficiency for this mutant relative to baseline), and $p = 0.114$ for $G4_2S$.

sensitivity to Arbidol with close to 20-fold inhibition at 4.9 μM Arbidol, the lowest concentration tested (compared to ∼4-fold inhibition of WT at this concentration). The effect of the stabilizing $K58_2I$ mutation did not follow the resistance pattern of the remainder of the X31HA-based panel. Significant inhibition was observed for the $K58_2I$ mutant at an intermediate Arbidol concentration and which had no effect on the destabilized mutants, but the mutant was inhibited less than WT. The seeming discrepancy in the resistance phenotype for the $K58_2I$ mutant might result from its location on the HA structure adjacent to the Arbidol binding site where it is likely to reduce the Arbidol binding affinity (Figure 1C).

Udorn HA-based panel showed a similar pattern of resistance to that observed for X31HA viruses with one notable exception (Figure 1E). In accord with results for X31HA viruses, WT Udorn was fully resistant, and this phenotype was reversed by the stabilizing $S4_2G$ mutation. We observed no additional effect of destabilizing mutations ($D112_2A$ and $H17_1R$) in the context of Udorn HA. Interestingly, the stabilizing $K58_2I$ mutation resulted in greater Udorn HA-virus sensitivity to Arbidol but not to the same extent as the $S4_2G$ mutation and resembled the phenotype of the X31HA $K58_2I$ virus. Most notably, the $H17_1Y$ mutation in Udorn HA did not reverse the resistance phenotype of WT Udorn. We interpret the $H17_1Y$ Udorn HA phenotype to result from the dominant effect of the destabilizing $S4_2$ over the stabilizing $Y17_1$ and expand upon this interpretation later (see the Discussion section). In sum, our results show that Arbidol sensitivity for the most part correlates with HA stability in or near the fusion peptide, with destabilizing mutations conferring resistance and stabilizing mutations conferring greater sensitivity to Arbidol during infection.

We sought to distinguish between three plausible mechanisms for the observed resistance or sensitivity to Arbidol by HA mutants. One possibility was that HA destabilization compensated for Arbidol effects by increasing the overall rate of fusion even when a fraction of HAs are slowed down or unable to participate due to Arbidol binding. However, this interpretation did not seem likely in the context of our previous conclusion that rate changes during endosomal fusion are inconsequential for infectivity.[16] A second possibility was that destabilizing HA mutations altered the Arbidol binding site allosterically. Finally, the destabilized HAs might permit Arbidol binding but resist its stabilizing effects at the pH of fusion.

To dissect the mechanism of Arbidol resistance for HA mutants, we performed total internal reflection fluorescent (TIRF)-based experiments of membrane fusion, which permit measurements of both the rate and efficiency of membrane fusion at the single-virion level (Figure 2A). We chose two resistant ($D112_2A$ and $G4_2S$) and the more sensitive ($H17_1Y$) X31HA viruses for the detailed analyses. Viruses were preincubated with Arbidol and then allowed to bind to the supported lipid bilayer incorporating sialic acid receptors and a pH-sensitive dye fluorescein. Fusion was triggered by introducing low-pH buffer containing Arbidol into the flow cell and monitored by fluorescence dequenching of the lipophilic DiD dye incorporated in the viral membrane (see

https://doi.org/10.1021/acsinfecdis.2c00178
ACS Infect. Dis. 2022, 8, 1543−1552

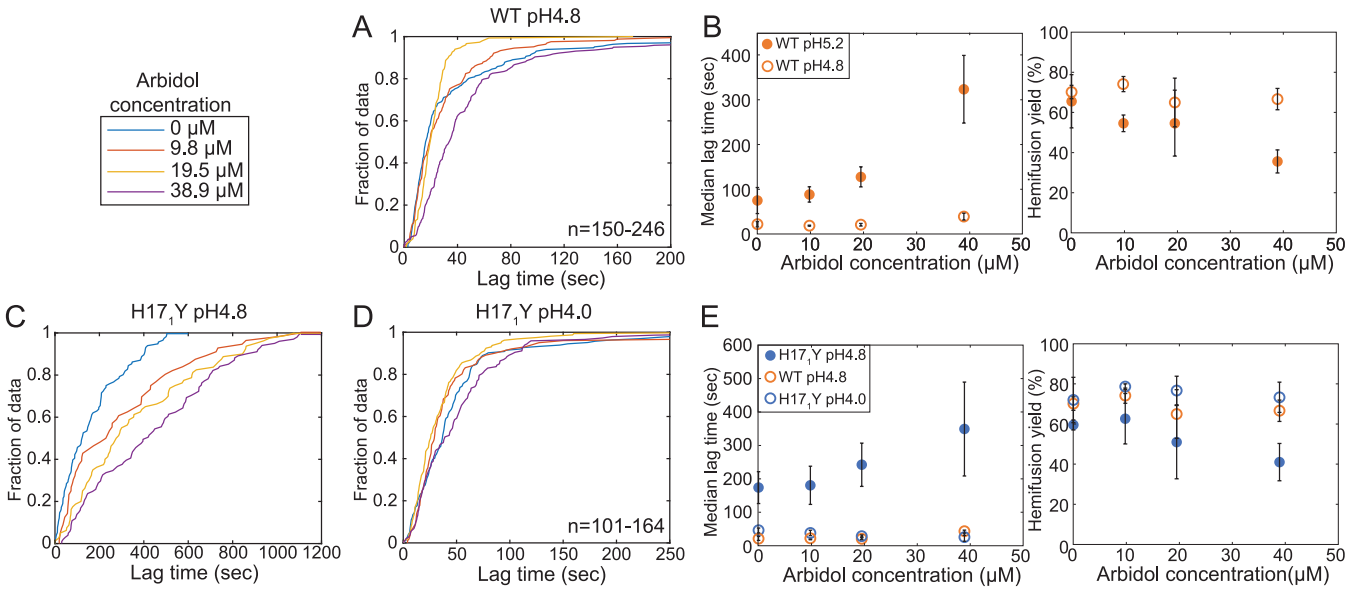

Figure 3. Sensitive viruses resist inhibition by Arbidol at sufficiently low pH. (a, b) WT X31HA virus hemifusion at pH 4.8. Cumulative distributions of hemifusion lag times for a representative set of experiments (a) and median hemifusion lag times (left) and yield (right) shown as the average ± standard deviation (b). The pH 5.2 data is also shown in Figure 2E. The *p*-values from a one-sided Student's *t*-test comparing median lag times of untreated to treated samples for WT virus at pH 4.8 are significant only for 38.9 μM Arbidol (p = 0.019). The *p*-value comparing hemifusion yield for WT virus at pH 4.8 between the untreated and 38.9 μM Arbidol is not significant, p = 0.192. (d, e) H17$_1$Y X31HA virus hemifusion. Cumulative distributions of hemifusion lag times at pH 4.8 (c) or pH 4.0 (d) for a representative set of experiments, and median hemifusion lag times (left) and yield (right) shown as the average ± standard deviation (e). The *p*-values from a one-sided Student's *t*-test comparing median lag times of untreated to treated samples for H17$_1$Y X31HA virus at pH 4.8 are significant only for 19.5 μM (p = 0.03) and 38.9 μM Arbidol (p = 0.003). Hemifusion lag times for H17$_1$Y X31HA virus at pH 4 are somewhat shorter for 19.5 μM (p = 0.01) and 38.9 μM Arbidol (p = 0.04). The p-values comparing the hemifusion yield for H17$_1$Y X31HA virus between the untreated and 38.9 μM Arbidol at pH 4.8 is $p = 5.4 \times 10^{-4}$, and at pH 4 is not significant, p = 0.43.

Videos S1−S10). We extracted the time delay for individual virions from the time of fluorescein dissipation to hemifusion (Figure 2). We determined hemifusion yield as the fraction of detected virions that underwent hemifusion in each field of view within 20 min of observation (Figure 2E). The 20 min mark was chosen as the cutoff because a clear decay in the frequency of hemifusion events was observed by this time for even the slowest of mutants at the highest Arbidol concentration, suggesting that measurements approached true hemifusion efficiency in all cases (Figures 2 and 3). In the presence of Arbidol, hemifusion lag-time distributions at pH 5.2 shifted toward slower times for the WT but remained unchanged for the destabilized mutants (Figure 2B−E and Videos S1−S4). Furthermore, hemifusion yield was significantly reduced for WT virus at the highest Arbidol concentration but was not decreased for the destabilized mutants (Figure 2E). The decrease in hemifusion efficiency for WT virus at pH 5.2 is consistent with Arbidol preventing rather than slowing down the conformational change of bound WT HAs[6,16] (Figure 2E). The unchanged rate or efficiency of hemifusion for the destabilized mutants confirms true resistance rather than compensation by the overall faster hemifusion rate by destabilized HAs (Figure 2C−E). Together, our single-virion fusion experiments showed that Arbidol prevents the low pH-induced conformational changes of WT HA, and HA destabilization near the fusion peptide confers resistance to Arbidol.

Our previous single-virion membrane fusion experiments related the pH dependence of the fusion rate to the probability that HA2 extends while HA1 remains in the open state.[6] In this model, the probability of HA2 extension in a given time window is related to the stability of the fusion peptide in its prefusion pocket, and the time that HA1 spends in the open state is determined by pH. The pattern of sensitivity and resistance to Arbidol by WT and mutant viruses (Figure 2) suggests that Arbidol delays WT but not destabilized HA2 extension past the window of opportunity provided by HA1 opening. The destabilized HAs might nonetheless be bound by Arbidol, but Arbidol might not prevent their extension at low pH. To probe whether HA destabilization is sufficient for allowing the evasion of Arbidol's effects, we performed single-virion membrane fusion experiments with WT X31HA virus in the presence of Arbidol at pH 4.8. We chose pH 4.8 because it represents the threshold pH, below which the rate of WT X31HA conformational changes is no longer pH-dependent and thus no longer limited by HA1 opening.[6,7] Furthermore, the hemifusion rate of WT IAV below pH 4.8 approximates that of destabilized mutants, suggesting that pH in this range destabilizes fusion peptides to a similar extent as the destabilizing mutations, and/or it destabilizes them sufficiently so that a different HA transition becomes rate-limiting.[6] We found that the WT X31HA virus resists inhibition by Arbidol at pH 4.8 and displays a pattern of resistance indistinguishable from that of destabilized mutants at pH 5.2 (Figure 3A,B and compare to Figure 2B−E; Videos S5 and S6 and compare to Videos S1−S4). Since WT HA is bound by Arbidol at neutral pH, this result is consistent with our interpretation that HA destabilization near the fusion peptide is sufficient to explain resistance to Arbidol.

To verify that the observed resistance of WT virus at pH 4.8 is owed to HA destabilization directly and not to the inability of Arbidol to bind to the prefusion HA at the lower pH, we

https://doi.org/10.1021/acsinfecdis.2c00178
ACS Infect. Dis. 2022, 8, 1543−1552

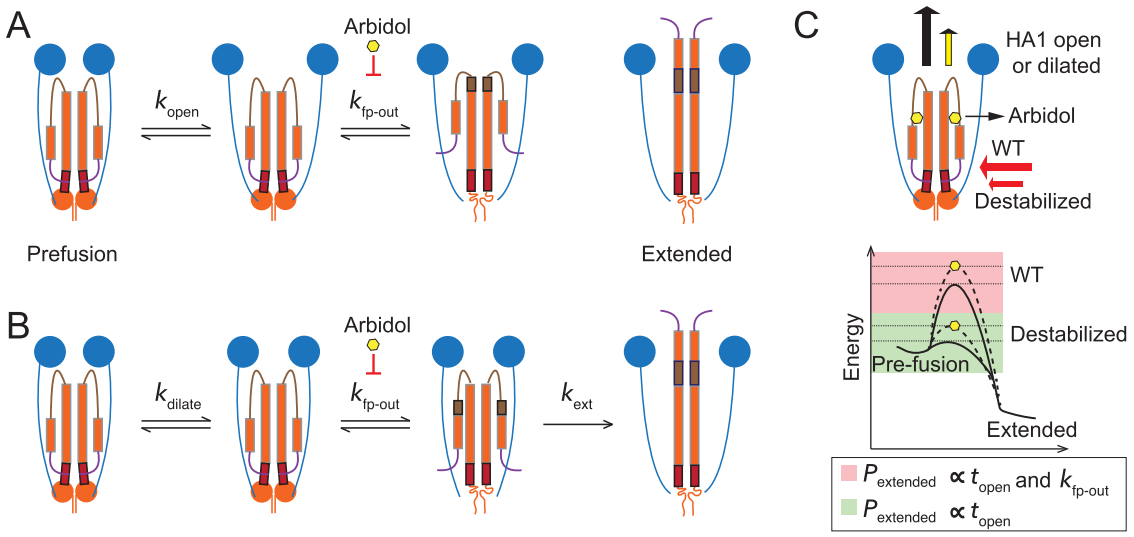

Figure 4. Updated model of the fusion-associated HA conformational dynamics and the mechanism of Arbidol resistance. (a, b) Low pH increases the average time that HA spends in the open or dilated state. The probability of HA2 extension is related to the free energy released by partial B-loop coiling, either by C-helix (coiled-coil) extension (a) or by A-helix extension (b), and the stability of the fusion peptides on prefusion HA2 during the window of opportunity afforded by HA1 head separation. (c) Complete HA extension is thermodynamically favorable but passes a kinetic-energy barrier imposed by the fusion-peptide release. Arbidol increases the free-energy penalty for B-loop coiling delaying extension (reduces the tug on the fusion peptide represented by the smaller upward arrow). Fusion-peptide destabilization by mutation or pH lowers the free-energy penalty for its release (smaller, side red arrow) allowing coiled-coil extension during the HA1 open state despite Arbidol binding to prefusion HA. In IAV with WT HA at the pH of endosomes, the probability of HA2 extension ($P_{extended}$) is related to the time that HA1 spends in the open or dilated state (t_{open}) and the rate of fusion-peptide release (k_{fp-out}) (red shaded region on the energy diagram). When fusion peptides are sufficiently destabilized, $P_{extended}$ solely relates to t_{open} and is insensitive to small changes in k_{fp-out} such as those resulting from Arbidol binding (green-shaded region).

performed single-virion fusion experiments with the stabilized $H17_1Y$ X31HA mutant virus at pH 4.8. Hemifusion by $H17_1Y$ X31HA mutant virus at pH 4.8 approximates that of WT X31HA virus at pH 5.2 in both rate and efficiency[16] (Figure 3C,E and compare to Figures 2B and 3B). Importantly, $H17_1Y$ X31HA mutant virus at pH 4.8 displayed a similar degree of sensitivity to Arbidol as WT virus at pH 5.2 in both hemifusion rate and yield effects. This result demonstrates that Arbidol retains the ability to bind to and inhibit the conformational changes of $H17_1Y$ X31HA at pH 4.8 (see also Videos S7 and S8 and compare to Videos S1, S2, S5, and S6). Our combined results (Figures 2 and 3) argue that resistance of destabilized mutants at pH 5.2 and of WT X31HA virus at pH 4.8 is at least, in part, owed to HA destabilization directly. Even the $H17_1Y$ X31HA mutant virus acquired resistance to Arbidol upon further pH reduction to 4 (Figure 3D,E and Videos S9 and S10), demonstrating fundamental similarity among Arbidol's effects against our panel of viruses that correlates with fusion-peptide stability. Our combined results offer direct support for and extend the fusion model we proposed previously[6] (see the Discussion section). Furthermore, our results reveal a mechanism of drug resistance deriving from a functional modification of its target rather than from mutation of the drug-binding site.

DISCUSSION

The current gold standard in antiviral inhibitor design is to target the conserved, functionally constrained epitopes on essential viral targets. However, mechanisms that modulate viral functions in ways that render inhibitor effects inconsequential for infectivity would represent a powerful evolutionary strategy ultimately forcing us to rework our own design standards. Our experiments with IAV and Arbidol have identified one such viral evasion strategy. Arbidol binds to a conserved site on HA and inhibits the extension of the HA coiled-coil for susceptible viruses. Destabilization of the fusion peptides by mutation or pH renders viruses resistant and permits unaltered fusion kinetics in the presence of Arbidol. The resistance phenotype is a direct function of fusion-peptide stability and need not evoke the absence of Arbidol binding to the prefusion HA (Figure 3). Arbidol experiments further extend our mechanistic picture of the HA-mediated membrane fusion (Figure 4).

The question of HA conformational sequence at low pH has been a matter of debate in the field. Classic work by Carr and Kim led to the "spring-loaded" model of HA-mediated membrane fusion, whereby the release of HA1 clamp from HA2 in open HA allows HA2 extension driven by the coiled-coil extension (B-loop-to-helix transition in Figure 1A).[38] This notion was supported by experiments showing that the inhibition of HA1 opening by engineered disulfide bridges prevents fusion-peptide exposure and inhibits membrane fusion.[3,4] However, recent biophysical and theoretical explorations have brought that notion into question and suggested that the fusion-peptide release might precede HA1 opening and coiled-coil extension.[18−23] Recent cryo-EM structures revealing conformational intermediates of the X31HA ectodomain at pH 5 show data consistent with the fusion-peptide release in the context of partial HA1 opening (i.e., dilation), also accompanied by the partial B-loop coiling extending the A-helix (B-loop end opposite the C-helix coiled-coil; see Figure 1A).[17] These data thus offer yet another alternative sequence of conformational transitions at least in the context of the free HA ectodomain at pH 5. In what follows, we discuss the questions of HA conformational

https://doi.org/10.1021/acsinfecdis.2c00178
ACS Infect. Dis. 2022, 8, 1543−1552

sequence and dynamics in the context of our new single-virion experiments with HA mutants in the presence of Arbidol.

Our current experiments offer insight into the sequence of HA conformational changes by coupling interpretations of its dynamics to quantitative measurements of membrane fusion and can thus reveal functionally relevant pathways. We found that destabilization of the fusion peptide can offset HA stabilization by Arbidol. Arbidol links B-loop from one HA2 monomer to the C-helix of an adjacent monomer where it must interfere with B-loop coiling that extends either the coiled-coil (Figure 4A) or A-helix (Figure 4B) or both.[27] The dependence of Arbidol's effects on fusion-peptide stability is consistent with concerted HA2 conformational changes where HA2 coiling near the Arbidol binding site drives and does not follow the fusion-peptide release. The energy provided by the complete coiled-coil extension was estimated to be in the range of −40 to −75 kcal/mol at the pH of fusion,[39,40] which likely exceeds the energy required to break the stabilizing fusion-peptide interactions in the prefusion pocket. Indeed, completion of B-loop coiling is not necessary for fusion-peptide release as its interruption by proline mutations spanning its middle region in the $F63_2P/F70_2P$ double mutant permits fusion-peptide release and target membrane insertion.[41] Shortening of the B-loop by helix extension on either end would impose a strain on the fusion peptide in the prefusion pocket. According to our current model, HA2 extension is under kinetic control, and the delay in HA extension by Arbidol binding is not limiting when fusion peptides are sufficiently destabilized (Figure 4C).

By linking the rate to the probability of HA2 extension, our current experiments support and extend the model of HA conformational dynamics proposed previously.[6,9] We previously related the pH dependence of the fusion rate to the probability that HA2 extends while HA1 remains in the open state.[6] By delaying B-loop coiling specifically, Arbidol experiments help relate the relative kinetics of HA1 opening and HA2 extension and suggest that HA1 opening regulates not only the rate but also the probability of HA2 extension. In the WT case exemplified by X31HA, this probability is finely tuned to the relevant time scales of HA1 opening at the pH of endosomes and in association with target membranes, so that small perturbations in this balance not only delay but also disable HA triggering. pH threshold is thus the pH regime where the rate of HA2 extension just exceeds the relevant time scales of HA1 opening. In WT viruses, the balance of the two rates ensures HA2 extension and membrane fusion at physiologically relevant time scales but otherwise disables HA triggering.

Tight regulation of HA triggering might be critical to prevent premature HA inactivation by thermal or pH fluctuations away from the host but provides an opportunity for virus inhibition by small molecules, such as Arbidol. Consistent with this model would be an alternative strategy for resistance to treatments that delay HA extension by prolonging the HA1 open state. Indeed, an HA1 mutation $G218_1R$, residing within the interface between HA1 head domains where it might destabilize the closed state, also confers resistance to Arbidol[26] (see Figure S1 and Table S1). Further supporting this model for the regulation of HA triggering is our previous observation that the stabilized $H17_1Y$ X31HA mutant displays inefficient fusion at pH 5.2 even in the absence of external inhibition.[16] Lower probability of HA2 extension for the same time window of HA1 opening would limit the extent of fusion for this mutant similar to how Arbidol affects WT X31HA virus. The HA conformational dynamics we uncovered explains the large degree of overlap between Arbidol and amantadine resistance mutations[26,28,33,42] (see Figure S1 and Table S1). Mutations that either reduce the free-energy cost for fusion peptide release or prolong the HA1 open state for a given pH would enable fusion either at a higher pH or in the presence of Arbidol.

We observed a seeming discrepancy in the extent of inhibition of susceptible viruses by Arbidol between the cell-based and *in vitro* single-virion experiments. While there was only a modest decrease in hemifusion yield for WT X31HA virus at 19.5 μM Arbidol (Figure 2E), there was about a 3-log reduction in infectivity for this virus at the same Arbidol concentration (Figure 1D). One key difference is that our infectivity experiments measure the effects of Arbidol on multiple cycles of infection, while hemifusion efficiency is measured in a single reaction round. However, there might exist other effects that amplify the differences between the two assays, such as conditions that reduce the probability of fusion-peptide insertion into the target endosomal over the idealized synthetic membranes *in vitro* (e.g., a more crowded target membrane and/or a greater distance of the receptor-bound virions from the target membrane). Indeed, we previously observed a greater effect of HA base-binding neutralizing antibodies in even a single cycle of infection than on hemifusion yield in our single-virion platform.[16]

Infectivity experiments with Udorn HA mutants allowed us to probe the dominance hierarchy of mutational effects as it relates to Arbidol sensitivity. WT Udorn is resistant to Arbidol owing to its destabilizing $S4_2$ (Figure 1E). Indeed, the Udorn HA $S4_2G$ virus is sensitive to Arbidol and resembles the WT X31HA virus in both sensitivity (Figure 1E) and membrane fusion kinetics.[6] $H17_1Y$ mutation has different consequences in the two WT backgrounds. In the context of $G4_2$ on X31HA, $H17_1Y$ is strongly stabilizing[16,35] and confers greater sensitivity to Arbidol (Figures 1D, 3C, and 3E). However, $H17_1Y$ in the context of $S4_2$ on Udorn HA did not diminish Arbidol resistance (Figure 1E), suggesting that the destabilizing effect of $S4_2$ is dominant over the stabilizing effect of $Y17_1$. The main region conferring fusion-peptide stability thus resides deep in its binding pocket.

Base bnAbs also bind the prefusion HA and inhibit conformational changes at the pH of fusion. However, destabilization of the fusion peptides does not confer resistance in this case.[16] Greater effectiveness of base bnAbs might be owed to their larger footprint or their binding in the immediate periphery of the fusion peptides or both. Our work has thus identified a potential limitation of targeting the prefusion HA by small molecules. However, the potential for mutations that facilitate HA triggering to become relevant in the clinic will depend on the physiological importance of tight kinetic coupling between HA2 extension and HA1 opening. A potentially more effective alternative to inhibiting membrane fusion by inhibiting HA2 extension might be by promoting HA2 extension. This could be achieved by destabilizing the fusion peptide, promoting HA1 open state, and/or facilitating B-loop coiling. HAs triggered to assume the lowest-energy, postfusion state away from the membrane target would be permanently lost as fusion participants. Indeed, one such small molecule, C22, has been previously described and shown to inhibit membrane fusion *in vitro* though its mechanism remains unexplored.[43] HA mutations that kinetically compensate for

https://doi.org/10.1021/acsinfecdis.2c00178
ACS Infect. Dis. 2022, 8, 1543−1552

the effects of destabilizing treatments would result in lower fusion efficiency in endosomes and might eliminate functional compensation as a resistance strategy.

METHODS

Reagents. *Cells.* MDCK.2 (ATCC strain CCL-34) and human embryonic kidney 293T (HEK293T) cells (ATCC strain CRL-3216) were propagated in DMEM supplemented with 10% FBS in a humidified 37 °C incubator with 5% CO_2. All infections were performed in infection media (OptiMEM (Thermo Fisher Scientific) supplemented with 1 μg/mL TPCK-trypsin (Sigma-Aldrich)). 6-Bromo-4-((dimethylamino)methyl)-5-hydroxy-1-methyl-2-((phenylthio)methyl)-1*H*-indole-3-carboxylic acid ethyl ester monohydrochloride (Arbidol) (Sigma-Aldrich) was dissolved in ethanol at 10 mg/ml and diluted to target concentration in infection media.

Viruses. IAVs used in this study have HA from either A/Aichi/68(X31) or A/Udorn/72(Udorn) and the remaining segments from Udorn.[44] Viruses were propagated and purified as described previously.[16] In brief, viruses were passaged at a multiplicity of infection (MOI) of 0.001 PFU/cell except for $H17_1Y$, which was passaged at an MOI of 0.1. Viruses were passaged twice at the low MOI before a high-MOI infection of 12 PFU/cell and virus purification. After each infection step, the infected-cell supernatants were clarified by centrifugation at 1000*g* for 10 min. After the final, high-MOI infection, the clarified supernatants were centrifuged through a 20% sucrose cushion in HNE20 (20 mM HEPES, 150 mM NaCl, 0.2 mM EDTA, pH 7.4) at 100,000*g* for 2.5 h at 4 °C to concentrate and partially purify the virus. The viruses were then further purified by centrifugation through a 20−60% (w/v) sucrose gradient at 100,000*g* for 2.5 h. The prominent top band, enriched in spherical virions, was collected.[6,16] Second-passage viruses were used in plaque reduction assays (Figure 1), and purified spherical viruses were used in single-virion hemifusion experiments (Figures 2 and 3).

Infectivity Experiments. Second-passage viruses of indicated strains were preincubated with infection media with 0, 4.5, 9.8, or 19.5 μM Arbidol at room temperature for 1 h before virus attachment to confluent MDCK.2 cell monolayers. Virus concentration in preincubations was adjusted to about 2×10^{10}−2×10^{11} PFU/mL (the noted virus concentrations refer to the infectivity of the input sample before Arbidol treatment). The virus was then diluted 10-fold serially in infection media containing the same Arbidol concentration, and 100 μL of virus dilutions was added per well of a 6-well plate. Attachment was performed at room temperature for 1 h with shaking every 6 min. After attachment, cells were overlayed with OptiMEM containing 1 μg/mL TPCK-trypsin, 0.6% Oxoid Agar (Thermo Fisher Scientific), and the same Arbidol concentration was used in preincubations. The plates were incubated at 34 °C for 2 days before fixing with 3.7% formaldehyde in phosphate-buffered saline (PBS) (137 mM NaCl, 2.7 mM KCl, 10 mM Na_2HPO_4, 1.8 mM KH_2PO_4 pH 7.4) at room temperature for 30 min. The overlayed media was removed, monolayers were washed with PBS, and the plate was imaged in brightfield using a Keyence fluorescent microscope BZ-X800 (Keyence) equipped with a 2× objective (Keyence Plan Apochromat, 0.1 NA). Light intensity was adjusted to 25% and exposure to 1/3000 s. Wells containing 20−200 plaques were scanned, and separate images corresponding to different parts of the well were stitched together using BZX-800 Analyzer software (version 1.1.2.4) to assemble a full-well image version for counting. The experiment including an entire panel of viruses was repeated at least three times. Figure 1B,C shows a representative result of an experiment performed in three biological replicates.

Single-Virion Membrane Fusion Experiments. *Hemifusion Assay.* The experiment followed an established procedure with only slight modifications to include Arbidol (pre)treatment of virions.[16] In brief, 6 μg of the purified virus was labeled with 1,1′-dioctadecyl-3,3,3′,3′-tetramethylindodicarbocyanine and 4-chlorobenzenesulfonate salt (DiD, Thermo Fisher Scientific) at 10 μM for 1.5 h at room temperature in a 25 μL reaction. Liposomes consisted of 4:4:2:0.1:2×10^{-4} ratio of 1,2,dioleoyl-sn-glycero-3-phosphocholine (Avanti Polar Lipids), 1-oleoyl-2-palmitoyl-sn-glycero-3-phosphocholine (Avanti Polar Lipids), sn-(1-oleoyl-2-hydroxy)-glycerol-3-phospho-sn-3′-(1′-oleoyl-2′-hydroxy)-glycerol (ammonium salt) (18:1 BMP (R,R); Avanti Polar Lipids), bovine brain disialoganglioside GD1a (Sigma-Aldrich), and *N*-((6-(biotinoyl)amino)hexanoyl)-1,2-dihexadecanoyl-sn-glycero-3-phosphoethanolamine (biotin-X DHPE; Molecular Probes, Life Technologies). We included 18:1 BMP (R,R) because of a published report showing that it promotes fusion with synthetic membranes for IAV and is a lipid enriched in late endosomes, the sites of IAV membrane fusion in cells.[45,46] Planar bilayers were formed from 200 nm liposomes in channels of a PDMS flow cell using the vesicle spreading method.[47] Sialic acid on GD1a served to attach IAV virions to the bilayer. Fluorescein-conjugated streptavidin (Invitrogen) at 30 μg/mL was bound to the bilayer and served as a pH indicator. DiD-labeled virions (untreated or pretreated with Arbidol at room temperature for 30 min) were flowed into the channels and allowed to attach at room temperature for 10 min. Unbound virions were washed out using HNE20, and pH was dropped by flowing in the low-pH buffer at the indicated pH (10 mM citrate, 140 mM NaCl, 0.1 mM EDTA). The wash and the low-pH buffers contained Arbidol concentration matching the preincubation conditions. The flow of the low-pH buffer was adjusted to 60 μL/min for the first minute and then to 20 μL/min for the rest of the experiment. Hemifusion was monitored as DiD dequenching from individual virions. All experiments were performed at a 23 ± 0.5 °C ambient temperature.

Microscope Configuration. The excitation and imaging pathways were unchanged relative to our previous setup except for the camera.[16] Some of the movies were imaged using the original 512 × 512 pixel EM-CCD sensor (Model C9100-13; Hamamatsu) and some using a newer, 1024 × 1024 pixel EM-CCD sensor (Model C9100-24B; Hamamatsu). A 488 nm laser at 1−2 μW (Obis, Coherent) was used to excite fluorescein, and 647 nm laser at 0.5−1 μW (Obis, Coherent) was used to excite DiD. The exposure time was 0.4 or 0.5 s depending on the virus and Arbidol concentration.

Data Analysis and Statistics. All data analysis for single-virion experiments was performed using MATLAB (MathWorks). The pH-drop time and DiD-dequenching time for individual virions were derived, as described previously.[6,16] We determined hemifusion yield as the percentage of detected virions that hemifused within 20 min of the pH drop. Statistical analyses for infectivity measurements, hemifusion time, and hemifusion yield were performed using one-tailed (expecting inhibition or no effect) unpaired Student's *t*-tests (for comparing medians of several independent measurements),

https://doi.org/10.1021/acsinfecdis.2c00178
ACS Infect. Dis. 2022, 8, 1543−1552

assuming equal variances. The *P*-values are either listed (Figures 2 and 3) or designated using the following symbols (Figure 1): NS, $P > 0.05$; *$P < 0.05$, the null hypothesis was rejected at the 5% significance level; **$P < 0.01$, the null hypothesis was rejected at the 1% significance level; ***$P < 0.001$, the null hypothesis was rejected at the 0.1% significance level; ****$P < 0.0001$, the null hypothesis was rejected at the 0.01% significance level.

■ ASSOCIATED CONTENT

Supporting Information

The Supporting Information is available free of charge at https://pubs.acs.org/doi/10.1021/acsinfecdis.2c00178.

Legends to sample videos of single-virion hemifusion of WT and mutant viruses in the absence or presence of Arbidol, published Arbidol-resistant mutants, mutants used in this study, and amino acid sequence comparison between WT X31 and WT Udorn HAs (PDF)

Sample videos of single-virion hemifusion of WT and mutant viruses in the absence or presence of Arbidol (ZIP)

■ AUTHOR INFORMATION

Corresponding Author

Tijana Ivanovic − *Biochemistry Department, Brandeis University, Waltham, Massachusetts 02453, United States;* orcid.org/0000-0002-1527-2303; Email: ivanovic@brandeis.edu

Authors

Zhenyu Li − *Biochemistry Department, Brandeis University, Waltham, Massachusetts 02453, United States*

Tian Li − *Biochemistry Department, Brandeis University, Waltham, Massachusetts 02453, United States;* Present Address: Project Director at Keybio

Meisui Liu − *Biochemistry Department, Brandeis University, Waltham, Massachusetts 02453, United States;* Present Address: Medical Student at Harvard Medical School

Complete contact information is available at: https://pubs.acs.org/10.1021/acsinfecdis.2c00178

Author Contributions

Z.L. and T.L. contributed equally to this work. Z.L.: experiment design, acquisition of data, analysis and interpretation of data, and writing of the manuscript. T.L. and M.L.: experiment design, acquisition of data, analysis, and interpretation of data. T.I.: conception and design, experiment design, acquisition of data, analysis and interpretation of data, and writing of the manuscript.

Notes

The authors declare no competing financial interest.

■ ACKNOWLEDGMENTS

The authors thank Stephen C. Harrison (Harvard Medical School) for helpful discussions and comments on the manuscript. The authors acknowledge support from the NIH Director's New Innovator Award 1DP2GM128204 (to T.I.) and the NSF MRSEC DMR-1420382 (to T.I.).

■ ABBREVIATIONS USED

IAV, influenza A virus; HA, hemagglutinin; bnAbs, broadly neutralizing antibodies; TIRF, total internal reflection fluorescence

■ REFERENCES

(1) Chen, J.; Lee, K. H.; Steinhauer, D. A.; Stevens, D. J.; Skehel, J. J.; Wiley, D. C. Structure of the Hemagglutinin Precursor Cleavage Site, a Determinant of Influenza Pathogenicity and the Origin of the Labile Conformation. *Cell* **1998**, *95*, 409−417.

(2) Harrison, S. C. Viral membrane fusion. *Virology* **2015**, *479*−*480*, 498−507.

(3) Godley, L.; Pfeifer, J.; Steinhauer, D.; Ely, B.; Shaw, G.; Kaufmann, R.; Suchanek, E.; Pabo, C.; Skehel, J. J.; Wiley, D. C.; Wharton, S. Introduction of intersubunit disulfide bonds in the membrane-distal region of the influenza hemagglutinin abolishes membrane fusion activity. *Cell* **1992**, *68*, 635−645.

(4) Kemble, G. W.; Bodian, D. L.; Rosé, J.; Wilson, I. A.; White, J. M. Intermonomer disulfide bonds impair the fusion activity of influenza virus hemagglutinin. *J. Virol.* **1992**, *66*, 4940−4950.

(5) Carr, C. M.; Kim, P. S. A spring-loaded mechanism for the conformational change of influenza hemagglutinin. *Cell* **1993**, *73*, 823−832.

(6) Ivanovic, T.; Choi, J. L.; Whelan, S. P.; van Oijen, A. M.; Harrison, S. C. Influenza-virus membrane fusion by cooperative fold-back of stochastically induced hemagglutinin intermediates. *eLife* **2013**, *2*, No. e00333.

(7) Floyd, D. L.; Ragains, J. R.; Skehel, J. J.; Harrison, S. C.; van Oijen, A. M. Single-particle kinetics of influenza virus membrane fusion. *Proc. Natl. Acad. Sci. U.S.A.* **2008**, *105*, 15382−15387.

(8) Otterstrom, J. J.; Brandenburg, B.; Koldijk, M. H.; Juraszek, J.; Tang, C.; Mashaghi, S.; Kwaks, T.; Goudsmit, J.; Vogels, R.; Friesen, R. H. E.; van Oijen, A. M. Relating influenza virus membrane fusion kinetics to stoichiometry of neutralizing antibodies at the single-particle level. *Proc. Natl. Acad. Sci. U.S.A.* **2014**, *111*, E5143−E5148.

(9) Ivanovic, T.; Harrison, S. C. Distinct functional determinants of influenza hemagglutinin-mediated membrane fusion. *eLife* **2015**, *4*, No. e1004595.

(10) Mosley, V. M.; Wyckoff, R. W. G. Electron Micrography of the Virus of Influenza. *Nature* **1946**, *157*, 263.

(11) Badham, M. D.; Rossman, J. S. Filamentous Influenza Viruses. *Curr. Clin. Microbiol. Rep.* **2016**, *3*, 155−161.

(12) Vahey, M. D.; Fletcher, D. A. Low-Fidelity Assembly of Influenza A Virus Promotes Escape from Host Cells. *Cell* **2019**, *176*, 281−294.e219.

(13) Hutchinson, E. C.; Charles, P. D.; Hester, S. S.; Thomas, B.; Trudgian, D.; Martínez-Alonso, M.; Fodor, E. Conserved and host-specific features of influenza virion architecture. *Nat. Commun.* **2014**, *5*, No. 4816.

(14) Harris, A.; Cardone, G.; Winkler, D. C.; Heymann, J. B.; Brecher, M.; White, J. M.; Steven, A. C. Influenza virus pleiomorphy characterized by cryoelectron tomography. *Proc. Natl. Acad. Sci. U.S.A.* **2006**, *103*, 19123−19127.

(15) Wharton, S. A.; Calder, L. J.; Ruigrok, R. W.; Skehel, J. J.; Steinhauer, D. A.; Wiley, D. C. Electron microscopy of antibody complexes of influenza virus haemagglutinin in the fusion pH conformation. *EMBO J.* **1995**, *14*, 240−246.

(16) Li, T.; Li, Z.; Deans, E. E.; Mittler, E.; Liu, M.; Chandran, K.; Ivanovic, T. The shape of pleomorphic virions determines resistance to cell-entry pressure. *Nat. Microbiol.* **2021**, *6*, 617−629.

(17) Benton, D. J.; Gamblin, S. J.; Rosenthal, P. B.; Skehel, J. J. Structural transitions in influenza haemagglutinin at membrane fusion pH. *Nature* **2020**, *583*, 150−153. PubMed

(18) Das, D. K.; Govindan, R.; Nikić-Spiegel, I.; Krammer, F.; Lemke, E. A.; Munro, J. B. Direct Visualization of the Conformational Dynamics of Single Influenza Hemagglutinin Trimers. *Cell* **2018**, *174*, 926−937.e912. From NLM

(19) Fontana, J.; Steven, A. C. Influenza virus-mediated membrane fusion: Structural insights from electron microscopy. *Arch. Biochem. Biophys.* **2015**, *581*, 86−97.
(20) Benhaim, M. A.; Lee, K. K. New Biophysical Approaches Reveal the Dynamics and Mechanics of Type I Viral Fusion Machinery and Their Interplay with Membranes. *Viruses* **2020**, *12*, 413.
(21) Benhaim, M. A.; Mangala Prasad, V.; Garcia, N. K.; Guttman, M.; Lee, K. K. Structural monitoring of a transient intermediate in the hemagglutinin fusion machinery on influenza virions. *Sci. Adv.* **2020**, *6*, No. eaaz8822.
(22) Lin, X.; Noel, J. K.; Wang, Q.; Ma, J.; Onuchic, J. N. Atomistic simulations indicate the functional loop-to-coiled-coil transition in influenza hemagglutinin is not downhill. *Proc. Natl. Acad. Sci. U. S. A.* **2018**, *115*, E7905−E7913.
(23) Fontana, J.; Cardone, G.; Heymann, J. B.; Winkler, D. C.; Steven, A. C. Structural changes in Influenza virus at low pH characterized by cryo-electron tomography. *J. Virol.* **2012**, *86*, 2919−2929.
(24) Kallewaard, N. L.; Corti, D.; Collins, P. J.; Neu, U.; McAuliffe, J. M.; Benjamin, E.; Wachter-Rosati, L.; Palmer-Hill, F. J.; Yuan, A. Q.; Walker, P. A.; Vorlaender, M. K.; Bianchi, S.; Guarino, B.; De Marco, A.; Vanzetta, F.; Agatic, G.; Foglierini, M.; Pinna, D.; Fernandez-Rodriguez, B.; Fruehwirth, A.; Silacci, C.; Ogrodowicz, R. W.; Martin, S. R.; Sallusto, F.; Suzich, J. A.; Lanzavecchia, A.; Zhu, Q.; Gamblin, S. J.; Skehel, J. J. Structure and Function Analysis of an Antibody Recognizing All Influenza A Subtypes. *Cell* **2016**, *166*, 596−608.
(25) Chai, N.; Swem, L. R.; Reichelt, M.; Chen-Harris, H.; Luis, E.; Park, S.; Fouts, A.; Lupardus, P.; Wu, T. D.; Li, O.; McBride, J.; Lawrence, M.; Xu, M.; Tan, M. W. Two Escape Mechanisms of Influenza A Virus to a Broadly Neutralizing Stalk-Binding Antibody. *PLoS Pathog.* **2016**, *12*, No. e1005702.
(26) Brancato, V.; Peduto, A.; Wharton, S.; Martin, S.; More, V.; Di Mola, A.; Massa, A.; Perfetto, B.; Donnarumma, G.; Schiraldi, C.; Tufano, M. A.; de Rosa, M.; Filosa, R.; Hay, A. Design of inhibitors of influenza virus membrane fusion: synthesis, structure-activity relationship and in vitro antiviral activity of a novel indole series. *Antiviral Res.* **2013**, *99*, 125−135.
(27) Kadam, R. U.; Wilson, I. A. Structural basis of influenza virus fusion inhibition by the antiviral drug Arbidol. *Proc. Natl. Acad. Sci. U.S.A.* **2017**, *114*, 206−214.
(28) Leneva, I. A.; Russell, R. J.; Boriskin, Y. S.; Hay, A. J. Characteristics of arbidol-resistant mutants of influenza virus: implications for the mechanism of anti-influenza action of arbidol. *Antiviral Res.* **2009**, *81*, 132−140.
(29) Boriskin, Y. S.; Leneva, I. A.; Pécheur, E. I.; Polyak, S. J. Arbidol: a broad-spectrum antiviral compound that blocks viral fusion. *Curr. Med. Chem.* **2008**, *15*, 997−1005.
(30) Brooks, M. J.; Burtseva, E. I.; Ellery, P. J.; Marsh, G. A.; Lew, A. M.; Slepushkin, A. N.; Crowe, S. M.; Tannock, G. A. Antiviral activity of arbidol, a broad-spectrum drug for use against respiratory viruses, varies according to test conditions. *J. Med. Virol.* **2012**, *84*, 170−181.
(31) Pécheur, E.-I.; Borisevich, V.; Halfmann, P.; Morrey, J. D.; Smee, D. F.; Prichard, M.; Mire, C. E.; Kawaoka, Y.; Geisbert, T. W.; Polyak, S. J. The Synthetic Antiviral Drug Arbidol Inhibits Globally Prevalent Pathogenic Viruses. *J. Virol.* **2016**, *90*, 3086−3092.
(32) Blaising, J.; Polyak, S. J.; Pécheur, E. I. Arbidol as a broad-spectrum antiviral: an update. *Antiviral Res.* **2014**, *107*, 84−94.
(33) Steinhauer, D. A.; Wharton, S. A.; Skehel, J. J.; Wiley, D. C.; Hay, A. J. Amantadine selection of a mutant influenza virus containing an acid-stable hemagglutinin glycoprotein: evidence for virus-specific regulation of the pH of glycoprotein transport vesicles. *Proc. Natl. Acad. Sci. U.S.A.* **1991**, *88*, 11525−11529.
(34) Rott, R.; Orlich, M.; Klenk, H. D.; Wang, M. L.; Skehel, J. J.; Wiley, D. C. Studies on the adaptation of influenza viruses to MDCK cells. *EMBO J.* **1984**, *3*, 3329−3332.
(35) Thoennes, S.; Li, Z.-N.; Lee, B.-J.; Langley, W. A.; Skehel, J. J.; Russell, R. J.; Steinhauer, D. A. Analysis of residues near the fusion peptide in the influenza hemagglutinin structure for roles in triggering membrane fusion. *Virology* **2008**, *370*, 403−414.
(36) Russell, R. J.; Kerry, P. S.; Stevens, D. J.; Steinhauer, D. A.; Martin, S. R.; Gamblin, S. J.; Skehel, J. J. Structure of influenza hemagglutinin in complex with an inhibitor of membrane fusion. *Proc. Natl. Acad. Sci. U.S.A.* **2008**, *105*, 17736−17741.
(37) Byrd-Leotis, L.; Galloway, S. E.; Agbogu, E.; Steinhauer, D. A. Influenza hemagglutinin (HA) stem region mutations that stabilize or destabilize the structure of multiple HA subtypes. *J. Virol.* **2015**, *89*, 4504−4516.
(38) Carr, C. M.; Chaudhry, C.; Kim, P. S. Influenza hemagglutinin is spring-loaded by a metastable native conformation. *Proc. Natl. Acad. Sci. U.S.A.* **1997**, *94*, 14306−14313.
(39) Huang, Q.; Korte, T.; Rachakonda, P. S.; Knapp, E. W.; Herrmann, A. Energetics of the loop-to-helix transition leading to the coiled-coil structure of influenza virus hemagglutinin HA2 subunits. *Proteins* **2009**, *74*, 291−303.
(40) Huang, Q.; Sivaramakrishna, R. P.; Ludwig, K.; Korte, T.; Böttcher, C.; Herrmann, A. Early steps of the conformational change of influenza virus hemagglutinin to a fusion active state: stability and energetics of the hemagglutinin. *Biochim. Biophys. Acta* **2003**, *1614*, 3−13.
(41) Gruenke, J. A.; Armstrong, R. T.; Newcomb, W. W.; Brown, J. C.; White, J. M. New insights into the spring-loaded conformational change of influenza virus hemagglutinin. *J. Virol.* **2002**, *76*, 4456−4466.
(42) Daniels, R. S.; Downie, J. C.; Hay, A. J.; Knossow, M.; Skehel, J. J.; Wang, M. L.; Wiley, D. C. Fusion mutants of the influenza virus hemagglutinin glycoprotein. *Cell* **1985**, *40*, 431−439.
(43) Hoffman, L. R.; Kuntz, I. D.; White, J. M. Structure-based identification of an inducer of the low-pH conformational change in the influenza virus hemagglutinin: irreversible inhibition of infectivity. *J. Virol.* **1997**, *71*, 8808−8820.
(44) Ivanovic, T.; Rozendaal, R.; Floyd, D. L.; Popovic, M.; van Oijen, A. M.; Harrison, S. C. Kinetics of proton transport into influenza virions by the viral M2 channel. *PLoS One* **2012**, *7*, No. e31566.
(45) Gui, L.; Ebner, J. L.; Mileant, A.; Williams, J. A.; Lee, K. K. Visualization and Sequencing of Membrane Remodeling Leading to Influenza Virus Fusion. *J. Virol.* **2016**, *90*, 6948−6962.
(46) Kobayashi, T.; Beuchat, M. H.; Chevallier, J.; Makino, A.; Mayran, N.; Escola, J. M.; Lebrand, C.; Cosson, P.; Kobayashi, T.; Gruenberg, J. Separation and characterization of late endosomal membrane domains. *J. Biol. Chem.* **2002**, *277*, 32157−32164.
(47) Nollert, P.; Kiefer, H.; Jähnig, F. Lipid vesicle adsorption versus formation of planar bilayers on solid surfaces. *Biophys. J.* **1995**, *69*, 1447−1455.

https://doi.org/10.1021/acsinfecdis.2c00178
ACS Infect. Dis. 2022, 8, 1543−1552